JOURNAL OF GEOPHYSICAL RESEARCH, VOL. 106, NO. A11, PAGES 25,919-25,927, NOVEMBER 1, 2001

Magnetic field and electric current density distribution in the geomagnetic tail, based on Geotail data

P. L. Israelevich and A. I. Ershkovich
Department of Geophysics and Planetary Sciences, The Raymond and Beverly Sackler Faculty of Exact Sciences, Tel Aviv University, Ramat Aviv, Israel

N. A. Tsyganenko [1]
Laboratory for Extraterrestrial Physics, NASA Goddard Space Flight Center, Greenbelt, Maryland

Abstract. Analysis of Geotail magnetic data enables us to reveal the antisunward electric current flowing along the tail axis. To our knowledge, observation of this current has not been reported yet. Distributions of the magnetic field and electric current density (along with their dependencies on the tilt angle of the Earth's dipole and components of the interplanetary magnetic field) have been derived directly from Geotail data, without any ad hoc assumptions. Analysis of the electric current density distribution shows that, in addition to currents associated with the geomagnetic tail flaring, there is a current (tentatively identified as the Hall current) flowing antisunward along the tail axis. The total strength of this current is of the order of 1 MA. It closes through the midnight sector of the auroral zone resulting in field-aligned currents in the region of the Harang discontinuity.

1. Introduction

The midnight sector of the auroral zone is one of the key regions for ionospheric-magnetospheric coupling. Two convection cells merge near the midnight meridian resulting in the reversal of the convection direction. Ionospheric currents associated with the plasma convection are directed eastward and westward in the evening and morning sectors, respectively. In the midnight sector, both electrojets exist for the same local times, and the boundary between them is known as the Harang discontinuity [*Harang*, 1946]. In the evening sector, westward plasma convection (and hence eastward electrojet) corresponds to the northward electric field, whereas the electric field responsible for westward electrojet is directed southward. Hence the electric field reverses its direction at the Harang discontinuity [*Heppner*, 1972]. Measurements of the field-aligned currents [*Iijima and Potemra*, 1978] have shown that three sheets of the electric current accompany the Harang discontinuity under quiet geomagnetic conditions. This distribution of field-aligned currents in the night polar cap is shown schematically in Figure 1 (top). Two sheets of downward current enclose the upward electric current. The poleward current sheet is an extension of the Region 1 currents in the morning sector, and the current sheet at the equatorward side corresponds to the Region 2 of the field-aligned currents in the morning sector. These field-aligned currents close somewhere in the geomagnetic tail, where a generator of the current system is located (while the ionosphere is an electric load). If we assume that the magnetosphere is symmetric with respect to the XZ plane (containing the vector of the solar wind velocity and the Earth's magnetic dipole), the feasible way to close the field-aligned currents in the vicinity of the midnight meridian is to allow an antisunward current, flowing along the tail axis, as shown in bottom of Figure 1. The existence of such an axial current in the tail is not surprising: it may arise as a Hall current in the plasma sheet, caused by the cross-tail electric field. Since that field is directed predominantly from dawn to dusk (i.e., $E_y > 0$), and the north-south component of the magnetic field in the plasma sheet B_z is also positive, the Hall current, indeed, should be antisunward [*Podgorny et al.*, 1988; *Dubinin et al.*, 1988].

On the other hand, the antisunward field-aligned current near the midnight plane (if it is strong enough) would destroy the symmetry of the magnetic field with respect to the XZ plane. The magnetic field lines would become twisted, invalidating the simple pattern of the closure current sketched in Figure 1. Thus the existence of the axial electric current in the tail requires a special investigation. To our knowledge, no observations

[1] Also at Raytheon ITSS Corporation, Lanham, Maryland.

Paper number 2000JA900165.
0148-0227/01/2000JA900165$09.00

of that current have been reported yet, and this is not quite surprising. First, the axial current, if it really exists, is too weak to be observed in single crossings of the geomagnetic tail. Second, it cannot be obtained in single-fluid numerical MHD simulations, since it is Hall current, whose treatment requires, at least, a two-fluid MHD approach. A good way to reveal that current from data is to obtain a distribution of the electric current density in the geomagnetic tail using large amounts of magnetic field measurements taken during plasma sheet crossings. This is the main goal of the present paper.

2. Method

We use an approach which enabled us to calculate the distribution of the magnetic field and electric current density in the comet Halley coma [*Israelevich and Ershkovich*, 1994; *Neubauer et al.*, 1995]. The coordinate system used in this paper is the solar wind magnetospheric system (*GSWM*) defined as follows [*Tsyganenko et al.*, 1998]. The X axis is antiparallel to the observed vector of the concurrent solar wind velocity, and the Y axis is perpendicular to the Earth's magnetic dipole so that the XZ plane contains the dipole axis.

Consider a cross section of the geomagnetic tail at $x = x_0$, covered by a grid $\{y_j, z_k\}$. We assume that the magnetic field in the tail is the function of seven variables: three coordinates $\{x,y,z\}$, b_y and b_z components of the interplanetary magnetic field (IMF) (we neglect a possible dependence on the x component of the IMF), the tilt angle Ψ of the Earth's dipole, and the dynamic pressure of the solar wind p, so that $\mathbf{B} = \mathbf{B}(x, y, z, b_y, b_z, \sin\Psi, p)$. Next we assume that in a vicinity of a grid point (j, k) the magnetic field components can be approximated by the first-order terms of the Taylor series:

$$B_i(x,y,z,b_y,b_z,\sin\Psi,p) = B_i(x_0,y_i,z_j,0,0,0,\langle p\rangle) + \frac{\partial B_i}{\partial x}(x-x_0) + \frac{\partial B_i}{\partial y}(y-y_j) + \frac{\partial B_i}{\partial z}(z-z_k) + \frac{\partial B_i}{\partial b_y}b_y + \frac{\partial B_i}{\partial b_z}b_z + \frac{\partial B_i}{\partial \sin\Psi}\sin\Psi + \frac{\partial B_i}{\partial p}(p-\langle p\rangle), \quad (1)$$

where $\langle p\rangle$ is the average solar wind pressure.

Considering all magnetic field measurements

$$\{\mathbf{B}^{l,mes}(x,y,z)\}$$

in the vicinity of the grid point

$$(|x-x_0| \le \Delta_x, |y-y_j| \le \Delta_y, |z-z_k| \le \Delta_z)$$

, we obtain the values of B_i, $\partial B_i/\partial x$, $\partial B_i/\partial y$, $\partial B_i/\partial z$, $\partial B_i/\partial b_y$, $\partial B_i/\partial b_z$, $\partial B_i/\partial \sin\Psi$, $\partial B_i/\partial p$ at that point by minimizing the merit function

$$\sum_l \Big\{ \left[B_x^{l,\mathrm{mes}}(x,y,z) - B_x(x,y,z,...)\right]^2 + \left[B_y^{l,\mathrm{mes}}(x,y,z) - B_y(x,y,z,...)\right]^2 + \left[B_z^{l,\mathrm{mes}}(x,y,z) - B_z(x,y,z,...)\right]^2 \quad (2)$$

under the condition that the magnetic field is divergenceless

$$\frac{\partial B_x(x_0,y_j,z_k,0,0,0,\langle p\rangle)}{\partial x} + \frac{\partial B_y(x_0,y_j,z_k,0,0,0,\langle p\rangle)}{\partial y} + \frac{\partial B_z(x_0,y_j,z_k,0,0,0,\langle p\rangle)}{\partial z} = 0. \quad (3)$$

The conditional extremum of the merit function has

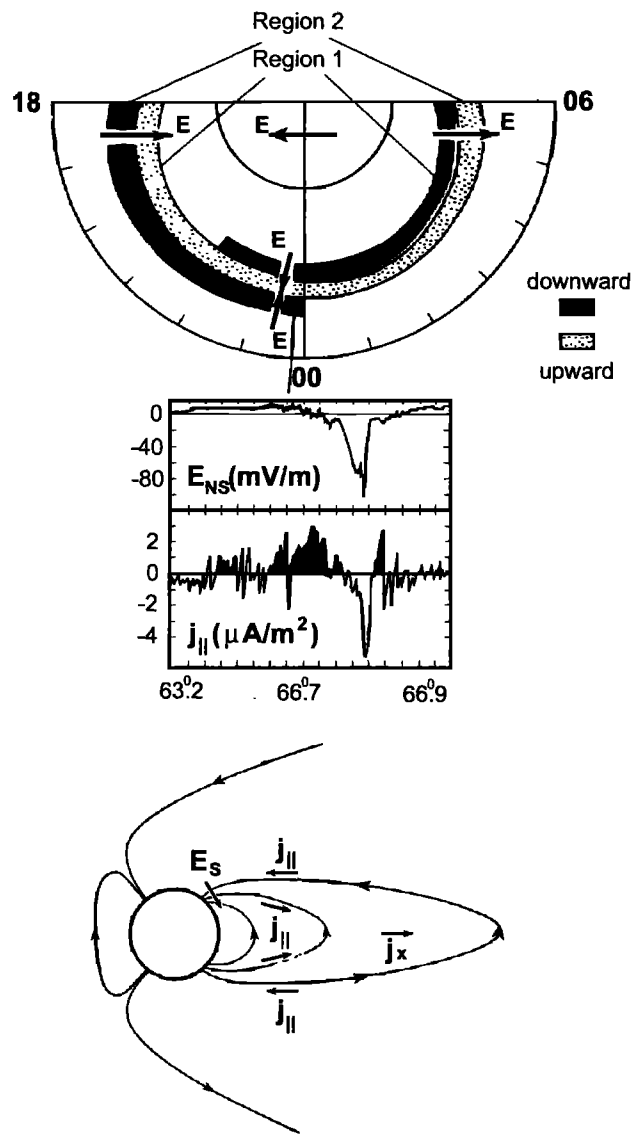

Figure 1. (top) Distribution of field-aligned currents in the nightside of the polar ionosphere. (middle) The electric field and field-aligned current density distribution along the midnight meridian [*Dubinin et al.*, 1988]. (bottom) A sketch of the midnight field-aligned currents closure through the geomagnetic tail.

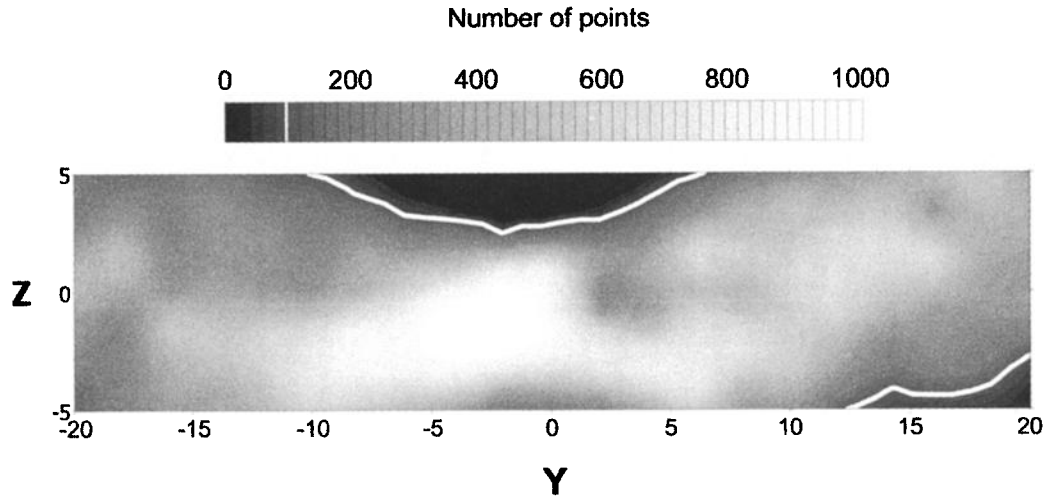

Figure 2. Distribution of the number of data points used for the calculation of the magnetic field and electric current at each grid point. White line shows the boundary of the region where the number of experimental points per grid cell was less than 100.

been found by using the Lagrange multipliers method. In this way, we immediately obtain the magnetic field in the entire cross section $x = x_0$, as well as the electric current density $\mathbf{j} = c/4\pi\nabla \times \mathbf{B}$, and (in the linear approximation) their response to the transverse components of the IMF, to the Earth's dipole tilt, and to the solar wind pressure.

We used the data set consisting of 5-min averages of Geotail magnetic field measurements, made in the geomagnetospheric tail during the period from January 1, 1993, to July 20, 1997. The measured magnetic field components were represented in the *GSWM* coordinates, and each data point was tagged by the concurrent values of the IMF b_y and b_z, the solar wind pressure, and tilt angle Ψ. Further details on the data set can be found elsewhere [*Tsyganenko et al.*, 1998].

The magnetic field distribution was calculated for the magnetotail cross section at $x = -20\,R_E$ within a rectangular area $|y| < 20\,R_E, |z| < 5\,R_E$), covered by a 21 × 21 grid with the cell size $2\,R_E$ by $0.5\,R_E$ in Y and Z directions, respectively. For each cell we used the data taken within a box $|x - x_0| \leq 10\,R_E$, $|y - y_j| \leq 1\,R_E$, and $|z - z_k| \leq 1\,R_E$. The size of data boxes in Z direction ($2\,R_E$) was intentionally assumed twice that for the cells ($1\,R_E$), so that each data point actually contributed to two adjacent cells and provided a "sliding" averaging of the data across the plasma sheet, which reduced irregular fluctuations in the resultant model field and current density. The density distribution of the data points over the grid is shown in Figure 2. Regions with a poor coverage by Geotail (with the number of data points per cell less than 100) are separated by a thick white line in the plot; the magnetic field distribution could not be accurately determined in those areas and hence those regions were eliminated from the study.

For each grid point the parameteres $\{a_i\} = \{x, y, z, b_y, b_z, \Psi, p\}$ are to cover more or less uniformly the parameter space near the point $b_y = 0$, $b_z = 0$. $\Psi = 0$, and $p = \langle p \rangle$. In order to check this requirement, we have calculated the average values of parameters $\langle a_i \rangle_{jk} = \sum a_{i,jk}/N_{ik}$ for each grid point $\{x_j, y_k\}$, their dispersion at each grid point $\sigma^2_{jk}(a_i) = \sum(a_{i,jk} - \langle a_i \rangle_{jk})^2/N_{jk}$, and compared the dispersion of average values $\sigma^2(\langle a_i \rangle_{jk}) = \sum_{j,k}(\langle a_i \rangle_{jk} - \langle\langle a_i \rangle_{jk}\rangle)^2/(NN \times MM)$ with the average value of dispersion $\langle \sigma_{jk}(a_i) \rangle = \sum_{j,k} \sigma_{jk}(a_i)/(NN \times MM)$. Here N_{jk} is the number of measurements near the grid node $\{x_j, y_k\}$, $NN \times MM$ is the total number of grid nodes, and $\langle\langle a_i \rangle_{jk}\rangle = \sum_{j,k} \langle a_i \rangle_{jk}/(NN \times MM)$.The results are listed in Table 1. The parameter space near the point $\{0, 0, 0, \langle p \rangle\}$ is covered uniformly if $\langle\langle a_i \rangle_{jk}\rangle < \sigma(\langle a_i \rangle_{jk}) < \langle \sigma_{jk}(a_i) \rangle$. One can see that this condition holds for the solar wind parameters (the IMF and the dynamic pressure). There is some violation of the coverage symmetry for the tilt angle due to the seasonal dependencies (the tilt angle is predominantly negative for Geotail crossings). Therefore we performed a special check for the tilt angle control of the magnetic field and electric current distributions (see Figure 5a and discussion in section 3).

Table 1. Comparison of Dispersion of Average Values With the Average Value of Dispersion

	$\langle\langle a_i \rangle_{jk}\rangle$	$\sigma(\langle a_i \rangle_{jk})$	$\langle \sigma_{jk}(a_i) \rangle$
b_y, nT	-0.10	0.60	2.90
b_z, nT	0.00	0.40	2.50
$\sin \Psi$	-0.19	0.17	0.17
$p - \langle p \rangle$, 10^{-8} dn cm^{-2}	0.00	15.60	66.50

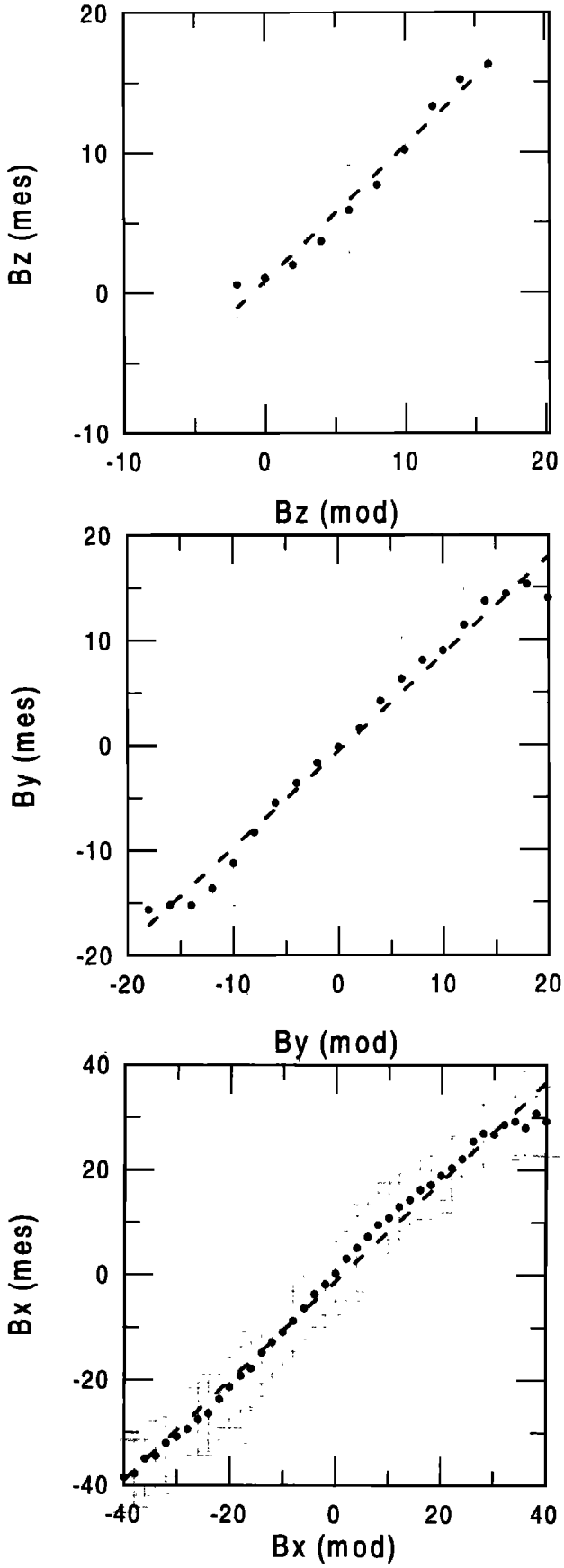

Figure 3. Measured magnetic field components against their calculated values.

3. Results

The calculated distributions of the magnetic field and electric current density components are shown in Plate 1 for $b_y = b_z = 0$, $\Psi = 0$, and $p = \langle p \rangle$. Our method was based on several simplifying assumptions of which the most serious one is the linear variation of the magnetic field components as functions of the variables $\{x, y, z, b_y, b_z, \Psi, p\}$. For that reason we need to verify our results. A simple verification method is to compare the values of the field components, predicted by (1), with the measured ones.

Figure 3 shows the plots of the measured magnetic field components B_i^{mes} against their values B_i^{mod}, calculated from (1) using the obtained set of values of the parameters B_i and $\partial B_i/\partial x_k$ at the grid nodes. Individual points in the plots correspond to the values of B_i^{mes}, averaged over 2 nT bins of B_i^{mod}, the vertical bars represent the data scatter, and the dashed lines are best linear fits. The agreement between the measured magnetic field components and their values, predicted by the discrete linear model (1), is fairly good. The correlation coefficients for B_x, B_y, and B_z components are 0.88, 0.8, and 0.7, respectively.

Another way to check the consistency of our results is to compare the values of the spatial derivatives $\{\partial B_i(y_j, z_k)/\partial x_m\}$, entering in (1) and obtained by minimizing the merit function (2), with those calculated directly from the node values $\{B_i(y_j, z_k)\}$ as, for example, $(B_i(y_j, z_{k+1}) - B_i(y_j, z_{k-1}))/2\Delta_z$. If our procedure is valid, then both values should be nearly equal. Figure 4 shows the scatterplot of the derivatives calcu-

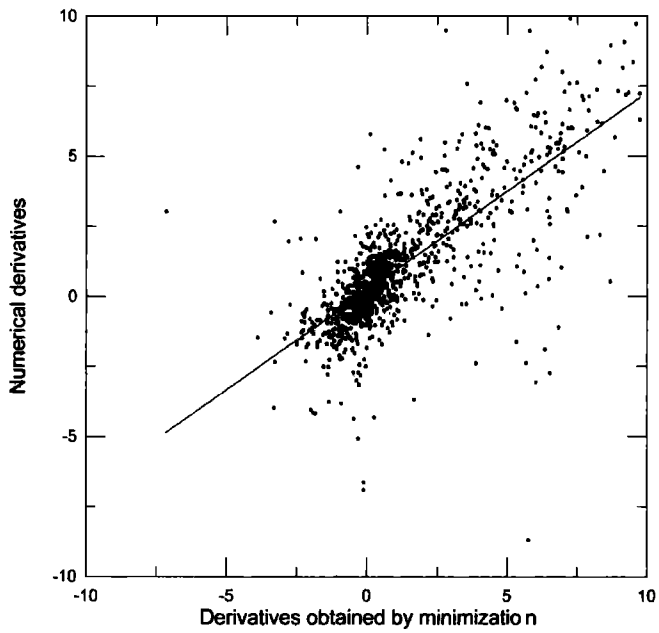

Figure 4. Magnetic field derivatives calculated from the magnetic field distribution $(B_i(y_j, z_{k+1}) - B_i(y_j, z_{k-1}))/2\Delta_z$ plotted against the derivatives $\partial B_i(y_j, z_k)/\partial z$ obtained by minimization of the merit function (2).

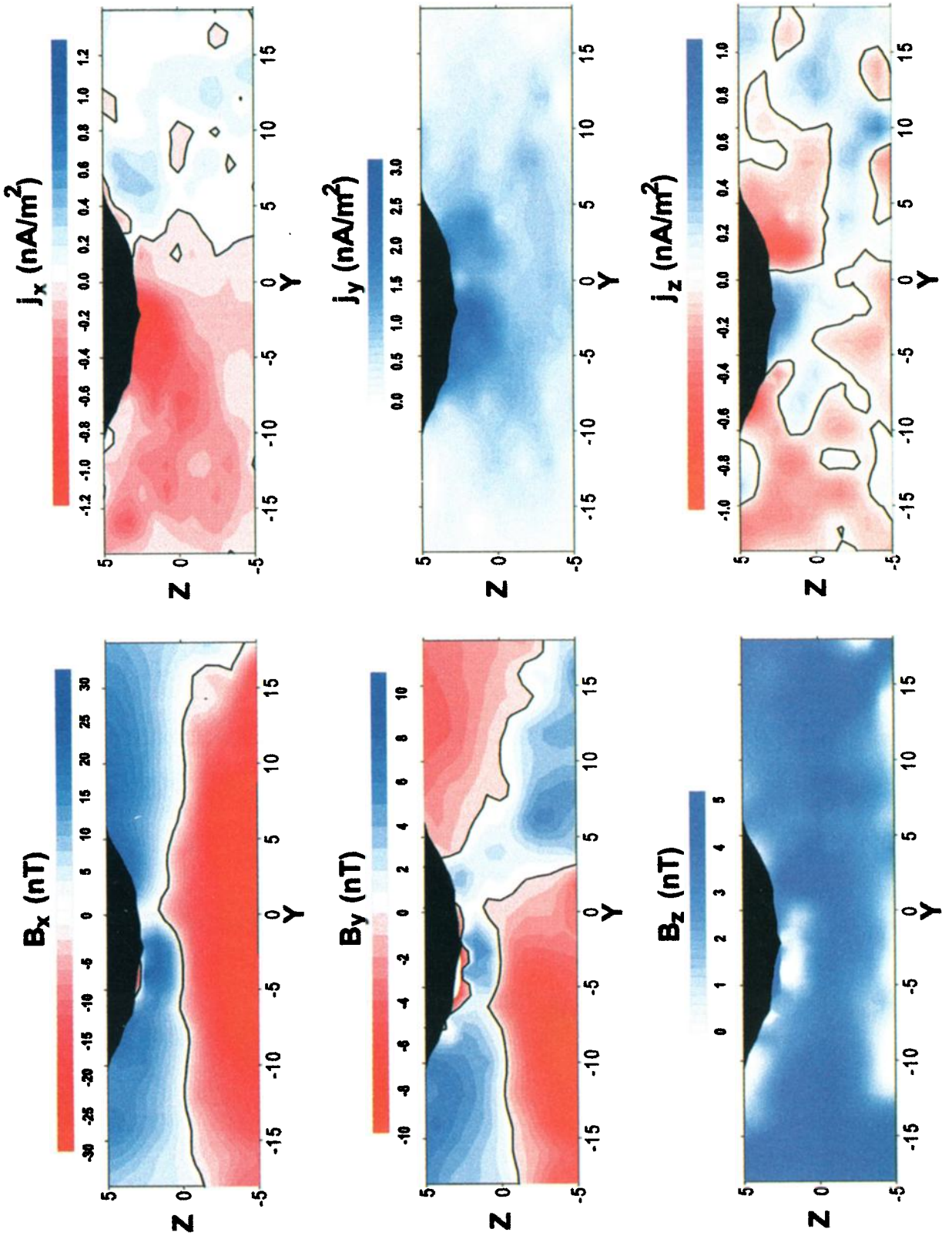

Plate 1. Calculated distributions of the (left) magnetic field and (right) electric current density components. For better viewing the color scales are different for each distribution.

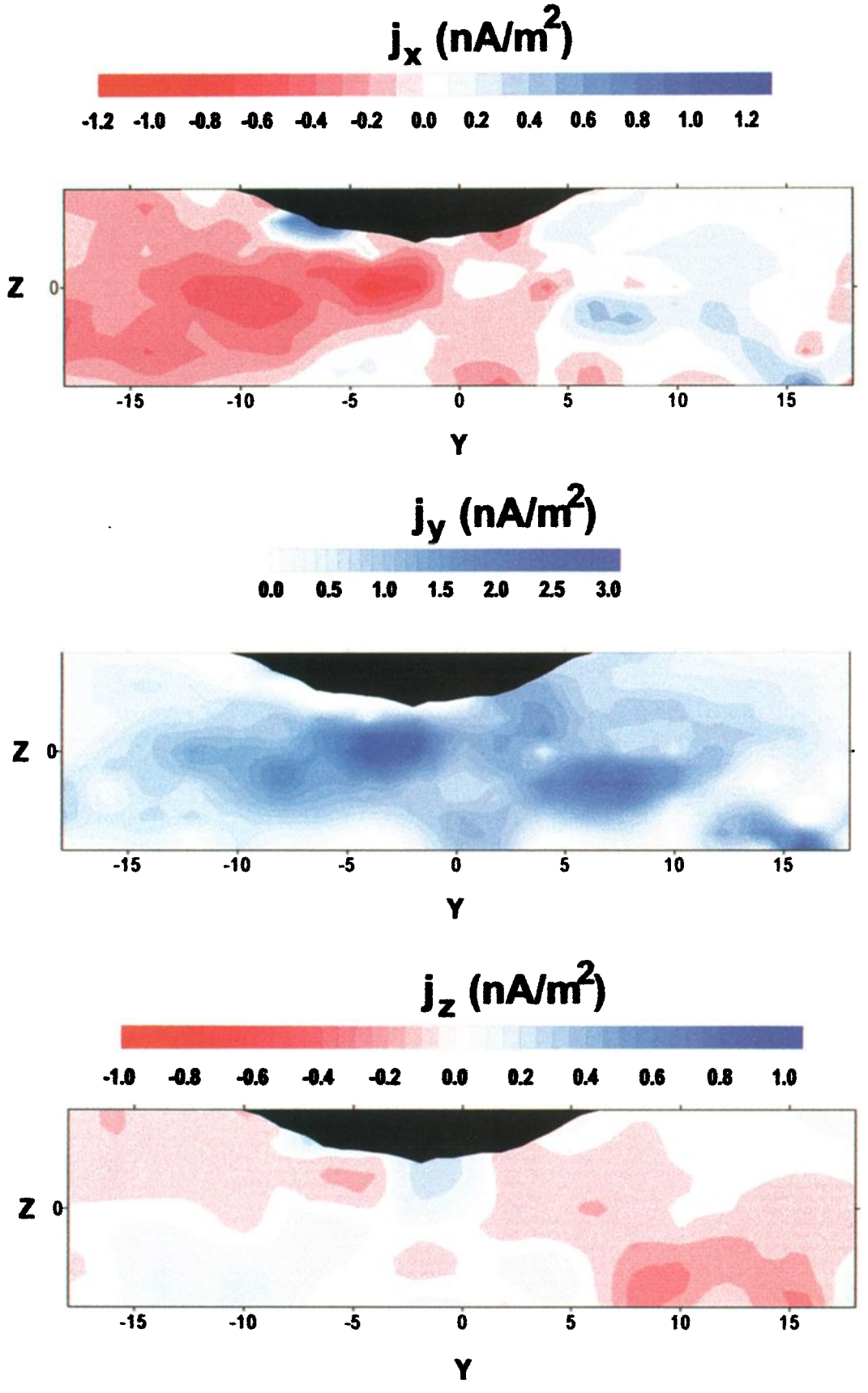

Plate 2. The distributions of the electric current density components calculated from the magnetic field distribution.

lated as $(B_i(y_j, z_{k+1}) - B_i(y_j, z_{k-1}))/2\Delta_z$ against the derivatives $\partial B_i(y_j, z_k)/\partial z$, obtained by minimizing (2). The two sets of derivatives agree fairly well, with the correlation coefficient $r = 0.8$. Plate 2 shows the electric current density calculated from the node values of $\{B_i(y_j, z_k)\}$ as curl **B** under assumption that $\partial/\partial x = 0$. Again, these distributions fairly well agree with the distributions obtained by minimizing the merit function (Plate 1).

Finally, knowing the node values B_i^{mod} and the derivatives $\partial B_i/\partial b_y$, $\partial B_i/\partial b_z$, and $\partial B_i/\partial \sin\Psi$ allows us to calculate the magnetic field distribution and hence the position and shape of the cross-tail current for any given values of the tilt angle Ψ and of the IMF b_y and b_z. The response of the tail current sheet to those parameters was addressed and revisited in many papers since early studies of the tilt-related warping [e.g., *Russell and Brody*, 1967] and of the IMF-induced twisting [*Russell*, 1972] of the tail current.

Both these effects are clearly observed in our model distributions. Figure 5a shows the position of the current sheet for $\Psi = -15^0$, and Figure 5b displays the twisting effect for $b_y = 5$ nT. (However, we did not find any significant effect of the IMF b_z upon the shape/position of the current sheet.) We compared these results with the warping/twisting effects found by *Tsyganenko et al.* [1998] from Geotail and ISEE 2 data. Dashed lines in Figure 5 show the current sheet position given by that model. Again, the agreement between the independently obtained results is fairly good. Hence we conclude that our results can be used for further analysis.

The distribution of the axial component j_x of the electric current density (Plate 1b) shows that there is an antisunward electric current along the tail axis. This current is significant compared to the background of the antisymmetric distribution of j_x with $j_x < 0$ for $y < 0$ and $j_x > 0$ for $y > 0$. The antisymmetric part of j_x is due to the geomagnetic tail flaring, manifested in the finite B_y component in the tail. For $z > 0$ the B_y component associated with the flaring is negative for $y > 0$, and positive for $y < 0$, while for $z < 0$ both B_x and B_y reverse their sign. This behavior of the B_y component can be clearly seen in Plate 1c. It corresponds to an antisymmetric distribution of j_x, so that $j_x < 0$ for $y < 0$ and $j_x > 0$ for $y > 0$. As clearly seen in Plate 1b, this symmetry is violated due to an additional antisunward current. As a result, the location of the reversal of the total j_x is shifted toward positive y, and the negative current at the morningside ($y < 0$) is nearly twice stronger than the positive one at the eveningside of the tail. The effect can also be seen in the plot of $j_x = j_x(y)$ (for $z = 0$), shown in the top panel in Figure 6 by a solid line. The bottom panel shows the result of separating the profile of j_x into antisymmetric (associated with the tail flaring) and symmetric parts (dashed and solid lines, respectively). The latter may be tentatively identified with the Hall current in the tail, which closes through the ionosphere near the midnight meridian and results in the electric current configuration, schematically shown in Figure 1.

The upper limit for the Hall current density can be roughly estimated by assuming that all ions entering in the tail plasma sheet remain unmagnetized (and hence do not participate in the earthward electric drift), while the electrons are fully magnetized. The resultant antisunward current in the central plasma sheet equals $j_x \sim necE_y/B_z$. Taking $E_y \sim 1.5 \times 10^{-4}$ V m^{-1}, corresponding to the potential drop of 50 kV across the tail width of $\sim 50\,R_E$, the plasma density $n \sim 0.1$ cm^{-3}, and $B_z \sim 1$ nT, we obtain the upper limit for the Hall current $j_x \sim 2.3$ nA m^{-2}, which does not contradict our model result $j_x \sim 0.5$ nA m^{-2}.

The total axial current I_x through the cross section obtained by the integration of our j_x distribution equals 1 MA. If one assumes that the entire current closes through the night sector of the ionosphere between 22 and 02 magnetic local time and the latitudinal width of the field-aligned current sheet is $\sim 1°$, the resultant volume density of the field-aligned current is 5 μA m^{-2}, in good agreement with the currents observed at low altitudes. Thus we conclude that the Geotail magnetic field data reveal the existence of the electric current, flowing along the geomagnetic tail axis and closing through the night sector of the auroral zone.

The antisunward Hall current along the geomagnetic tail axis should grow with the convection electric field E_y. This implies that the current should be stronger for negative interplanetary magnetic field, as the cross-tail potential drop increases. This effect can be clearly seen

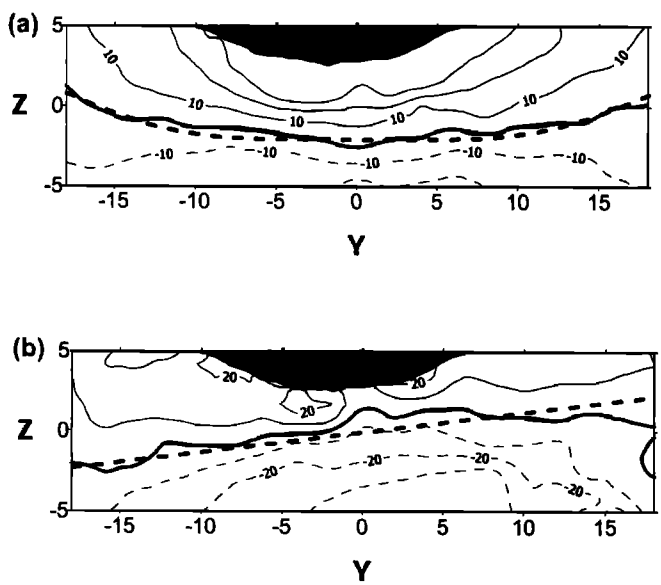

Figure 5. Distributions of the B_x component in the geomagnetic tail ($x = -20\,R_E$) for (a) the tilt angle $\Psi = -15^0$ and for (b) the IMF component $b_y = -5$ nT. Thick solid line shows the position of the neutral sheet. Dashed line corresponds to the neutral sheet position obtained in the model calculations of *Tsyganenko et al.* [1998].

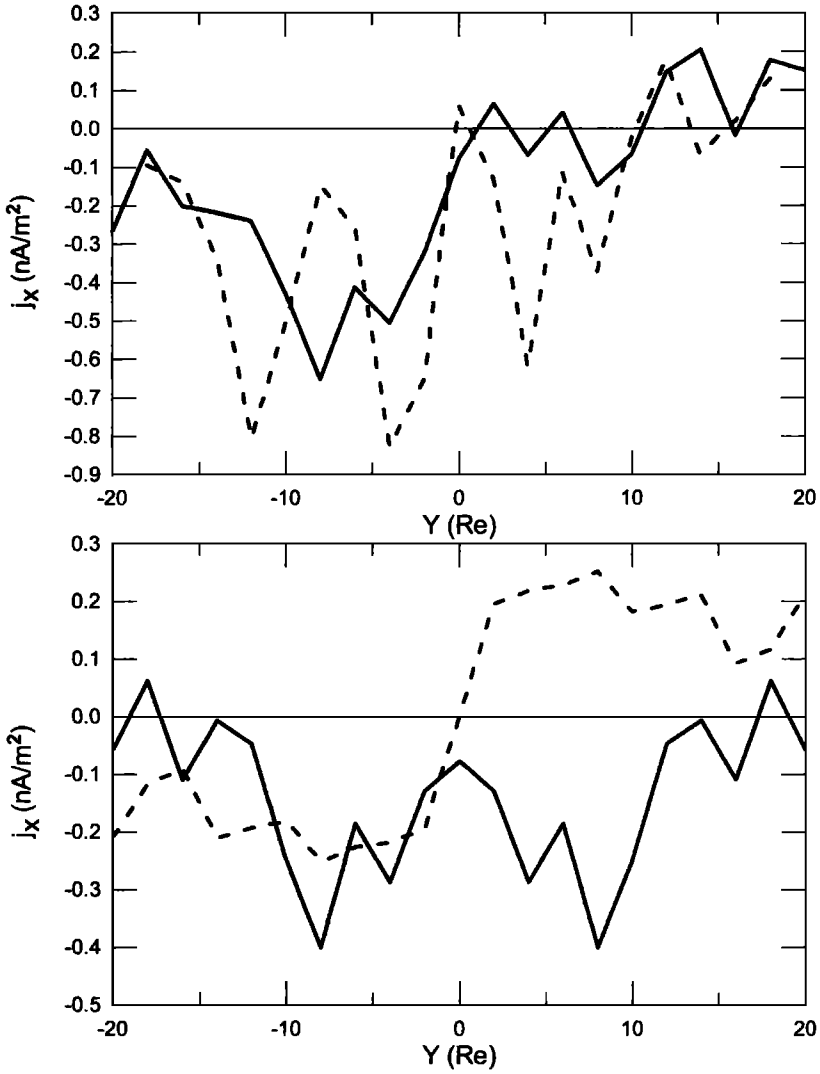

Figure 6. (top) Dawn-dusk profiles of the axial component of the electric current density $j_x(y)$ for $z = 0$. Solid line corresponds to the model distribution of the electric current density for IMF $b_z = 0$. Dashed line gives the same dependence for IMF $b_z = -5$ nT. (bottom) Symmetric (solid line) and antisymmetric (dashed line) parts of the model profile of $j_x(y)$ for IMF $b_z = 0$.

from the obtained distributions of the electric current density. We calculated j_x for different values of b_z from the distributions $\mathbf{B}(x_0, y_j, z_k, b_z) = \mathbf{B}(x_0, y_j, z_k, 0) + (\partial\mathbf{B}/\partial b_z)b_z$. Results for $b_z = -5$ nT are shown in the top panel of Figure 6 by dashed lines. The axial current density increases by 50%, as the IMF b_z drops from 0 to -5 nT.

4. Conclusion

Using Geotail magnetometer data, we obtained distributions of the magnetic field and electric current density and their response to both the tilt angle of the Earth's magnetic dipole and to the b_y and b_z components of the interplanetary magnetic field. These distributions have been derived directly from the data, without any ad hoc assumptions on the configuration of the electric current. Well-known features, such as the current sheet warping for tilted orientation of the geodipole and the current sheet twisting around the x axis, induced by the y component of the IMF, are reproduced correctly. The current sheet position is not affected by the b_z component of the IMF.

The distribution of the j_x component of the electric current density reveals both the current, associated with the geomagnetic tail flaring, and the antisunward Hall current. The axial antisunward current closes through the midnight sector of the auroral zone and corresponds to the upward field aligned current, observed near the Harang discontinuity.

Acknowledgments. The Geotail magnetic field data were kindly provided by Susumu Kokubun of the Institute Space and Astronautical Science (ISAS), Japan. The work of one of us (N.A.T.) was supported by NASA grant NASW-97024 (ISTP GI Program) and by the NSF Magnetospheric Physics Program grant ATM-9819873.

Michel Blanc thanks Malcolm Dunlop and another referee for their assistance in evaluating this paper.

References

Dubinin, E. M., P. L. Israelevich, N. S. Nikolaeva, I. M. Podgorny, A. K. Kuzmin, A. N. Zaitsev, and V. G. Petrov, Electrodynamics of the morning sector of the auroral oval, *Kosm. Issled., 26*, 890, 1988.

Harang, L., The mean field of disturbance of solar geomagnetic storms, *J. Geophys. Res., 51*, 353, 1946.

Heppner, J. P., The Harang discontinuity in auroral belt ionosphere currents, *Geophys. Publ., 29*, 105, 1972.

Iijima, T., and T. A. Potemra, Large-scale characteristics of field-aligned currents associated with substorms, *J. Geophys. Res., 83*, 599, 1978

Israelevich, P. L., and A. I. Ershkovich, Induced magnetosphere of comet Halley 2. Magnetic field and electric currents, *J. Geophys. Res., 99*, 21,225, 1994.

Neubauer, F. M., P. L. Israelevich, and A. I. Ershkovich. Two-dimensional and three-dimensional magnetic vector field distributions from Giotto encounter data for comparison with comet/solar wind interaction models, *SIMPO Newsl., 5*,(13), 3, 1995.

Podgorny, I. M., E. M. Dubinin, P. L. Israelevich, and N. S. Nikolaeva, Large-scale structure of the electric field and field-aligned currents in the auroral oval from the Intercosmos-Bulgaria-1300 satellite data, *Geophys. Res. Lett., 15*, 1538, 1988.

Russell, C. T., The configuration of the magnetosphere, in *Critical Problems of Magnetospheric Physics*, edited by E. R. Dyer, pp. 1 - 16, IUCSTP Secretariat, Nat. Acad. of Sci., Washington, D. C., 1972.

Russell, C. T., and K. I. Brody, Some remarks on the position and shape of the neutral sheet, *J. Geophys. Res., 72*, 6104, 1967.

Tsyganenko, N. A., S. B. P. Karlsson, S. Kokubun, T. Yamamoto, A. J. Lazarus, W. W. Ogilvie, C. T. Russell, and J. A. Slavin, Global configuration of the magnetotail current sheet as derived from Geotail, Wind, IMP 8 and ISEE 1/2 data, *J. Geophys. Res., 103*, 6827, 1998.

A. I. Ershkovich and P. L. Israelevich, Department of Geophysics and Planetary Sciences, The Raymond and Beverly Sackler Faculty of Exact Sciences, Tel Aviv University, Ramat Aviv 69978, Israel. (peter@jupiter1.tau.ac.il)

N. A. Tsyganenko, Code 690.2, Laboratory for Extraterrestrial Physics, NASA Goddard Space Flight Center, Greenbelt, MD 20771. (e-mail: kolya@nssdca.gsfc.nasa.gov)

(Received May 18, 2000; revised November 22, 2000; accepted November 26, 2000.)